

COMPUTATIONAL STUDIES OF FLUID FLOW AND PRESSURE DISTRIBUTIONS IN A SPIRAL GROOVE SEALS

Vladimir Kudriavtsev¹, M. Jack Braun² and Robert C. Hendricks³

vvk@cfdcanada.com, mbraun@uakron.edu, robert.c.hendricks@grc.nasa.gov

¹*Principal Engineer, CFD Canada / CERCA, Montreal*

²*Professor, University of Akron, Akron, Ohio*

³*Principal Scientist, NASA Glenn Research Center, Cleveland, Ohio*

Key Words: Spiral Groove Seal (SGS), CFD, load capacity, flow visualization, turbomachinery

ABSTRACT

The **Spiral Groove Seal** is a self-acting device that uses the fluid flowing between its faces to lift the sealing faces from each other. Thus, it is also referred to as a non-contacting face seal. In this paper we utilized a full 3D Navier-Stokes equations solver (CFD-ACE+) to study the flow patterns inside an inward pumping spiral groove seal. CFD-ACE+ (<http://www.cfdrc.com>) is a commercial software package that has inherited many advanced features implemented in a research code SCISEAL[1] developed by CFD Research Corporation for NASA Glenn (Lewis) Research Center (1992-96).

INTRODUCTION

The Spiral Groove Seal (SGS), a typical example of hydrodynamic self-acting device [2,3,4], is presently widely used by the industry in form of cylindrical seals [4], face mechanical seal [5], or even as a form of thrust bearing. The seal assembly of a typical SGS (face seal) is shown in Figs. 1 and 2. Here, the grooves on the outside portion of the stator are oriented such as to pump inward with the pressure gradient [6]. The inward pumping is produced, in this case by the clockwise motion of the rotor. The cylindrical seal version of the example shown in Figure 1 has the grooved pattern etched on the stationary cylindrical surface and the seal is divided into two areas. The first low pressure region has grooves that are optimized to produce a maximum stagnation pressure. Grooves are spatially oriented to produce a pumping component in the axial direction. Pressure will increase due to the pumping action and will partially offset the imposed pressure gradient between P_{high} and P_{low} sides [6]. The second region is smooth and serves as the seal dam. This region

works in conjunction with the grooved region. As the fluid is pumped through the grooves towards the dam, the pressure increases inside the spiral groove due to the interaction of the rotating flow with the groove sidewalls. Typically, the shaft(or disk) is rotating at speeds in excess of 10,000 rpm, with clearances between the rotating and stationary components below 0.001 inch. The SGSs have dual utilization and are now also actively pursued in advanced bearing designs [7]. The inward pumping spiral groove (face or cylindrical) creates a positive pressure gradient that causes the required sealing effect. The pumping characteristic is most critical and strongly depends on the rotational speed, direction of rotation, groove depth, orientation and shape, groove



Figure 1. Example of John Crane's Face Seal

to dam ratio and liquid/gas properties. Possible alternate groove layouts are shown in Fig. 3

Existing numerical simulations of SGS are limited mostly to Reynolds equation application [5-9]. However, very strong flow recirculation patterns take place in the groove/dam area (see Fig. 5) and flow formations can be rather complex[10]. Presently NASA developed computational models SPIRALI,

SPIRALG [4,6], Crane's CSTEDY [5] and others [9] are limited to narrow groove theory [4,11], and can not accurately consider effects of turbulence, inertia, non-isothermal flow, or flow choking [6]. Computational fluid mechanics (CFD) methods have been actively utilized to study 2-D and 3-D fluid flows in many advanced seals and bearings (Lauder[13], Braun/Dzodzo[14], Braun/Kudriavtsev[15], SCISEAL[1]). Despite some recent advances in spiral groove seal modeling [9,12] **no one** was able to solve 3-D flows and obtain pressure distributions in full Navier-Stokes formulation. This can be attributed to computational difficulties that arise at the gap/clearance and groove interfaces at high rotational speeds. Considerable 'grid stretching' (over 1:100) may be required to adequately resolve flows in these type of gaps. On the basis of the previous CFD work of the present authors we consider that it is presently feasible to utilize 3-D Navier-Stokes models for studies, design and optimization of the spiral groove seal.

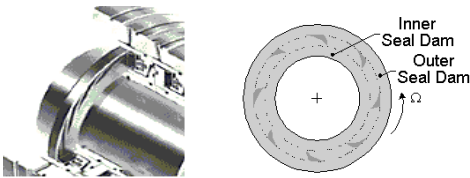


Figure 2. Generic Geometry [9]

MODEL SETUP

To design an efficient spiral groove device, one needs to optimize in tandem combination of parameters, most critical being groove depth, groove angle, groove width and the number of grooves along the circumference(that determines groove-to-land-ratio). In Fig. 3 we demonstrate 4 possible plane layouts for the spiralgroove computational setups. Groove angle can be aligned/or opposite to the direction of rotation and grooves can be converging or diverging. To these authors best knowledge, no studies were attempted to comparatively analyze groove layouts, compare 3-D flow formations, leakage and resulting pressure gradients. Here, grooves are on the stator while the rotor moves with speeds up to 40,000 rmp and a clearance between 0.0002 and 0.001 inch. Depending on the application, one optimal groove layout will emerge out of the four schematics presented in Fig. 3. In this study we will focus on a realistic generic geometry and will present resulting three-dimensional flows and pressure drops for diverging groove layout .

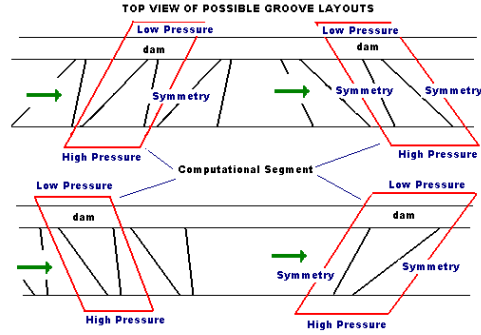


Figure 3. Case Studies of Possible Layouts
 Row1 : converging groove; Row2 : diverging groove
 Column1 : opposite rotation; column2 : aligned with rotation

Computational Configuration. The spiral groove seal section is shown in Fig. 4, and represents a diverging groove layout. Depending on the direction of rotation the groove angle is aligned with, or opposed to a pumping vector. The groove inlet is located at the high pressure end and the sealing dam (just like a Rayleigh step) is located at the low pressure end. Flow leaks from «inlet» to «outlet» due to the pressure differential and is also entrained into the groove area by the mechanical pumping action of the rotating shaft. We utilized a segment of real face seal ($R_{inner}=1.84 \text{ E-2m}$, $R_{outer}=5 \text{ E-2 m}$, clearance= 1E-5 m , groove depth $G_d=5\text{E-4 m}$ and a runner speed of $\omega=25,000 \text{ rpm}$ (2600 rad/s). P_{high} (outer diameter) at the inlet was $4.5\text{E}5 \text{ Pa}$ and P_{low} was equal $1\text{E}5$ (outlet, inner diameter). Due to cylindrical symmetry in the direction of rotation we utilized cyclic boundary conditions in the clearance area on the left and right boundaries (Fig. 4). These boundaries are also marked as «symmetry» on Fig. 3. Cyclic boundary condition means that left boundary outlet is used as inlet for the right boundary.

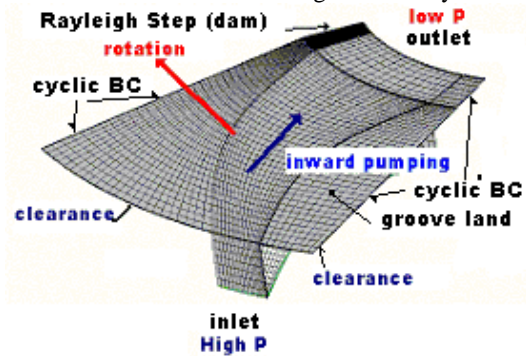


Figure 4. Generic Computational Setup –

Compressible laminar and $k-\epsilon$ turbulent flow models were utilized using CFD-ACE+ [16] developed by CFD Research Corporation. Gas properties followed Sutherland's formula for viscosity, ideal gas law for density (Mol.wt=29), $C_p=1000 \text{ J/kg-s}$. Rotational speed of 414 turns/sec was specified on the runner surface. Computational setup also allows to account for effects of groove angle/rotation alignment. This is done by changing sign of rotating velocity from positive to negative.

A structured multi-block computational grid was utilized, with 20,163 cells. Grid was partitioned on groove, dam, and 2 land areas (see Fig.4). A typical solution process required 350 iterations to converge 4 orders of magnitude for u,v,p , resulting in computational time of 45 min on a Pentium II 300MHz computer (Fig. 5).

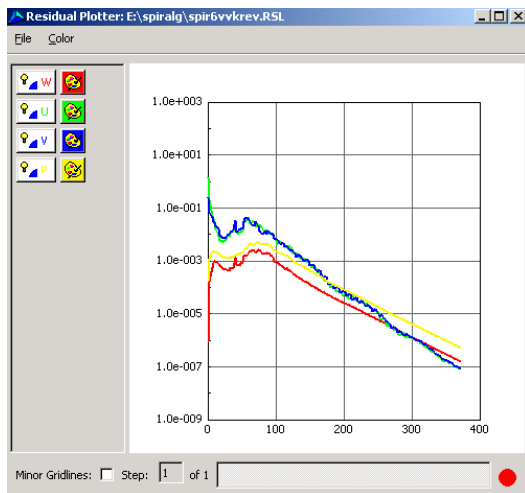


Fig. 5 Convergence plot, $\Delta P=3.5E5$ (51 psi) at 25,000 rpm

The computational model (grid, geometry, coordinate system) was developed using the advanced features of CFD-ACE+/GEOM that allows to create configurable physical model setups (GUI), and to link the parametric template-based gridding with the solver input parameters [17]. The resulting models become flexible application tools tailored for non-expert CFD users, and capable to perform a wide range of spiral groove design and optimization analysis (see Appendix 1).

RESULTS & DISCUSSION

The goals of this paper were three-fold. First, we intended to demonstrate feasibility of the full

Navier-Stokes solution for spiral groove seal configuration at realistic operating conditions. These conditions are : gap seal clearance $C < 0.001$ inch, seal inside diameter, $ID > 1$ inch, and angular velocities higher than 10,000 rpm. Secondly, we planned to demonstrate the complex 3-D nature of the flow in the seal, and by doing so to highlight the limitations of narrow groove [4,6] and Reynold's equations. Finally, authors compare performance of two alternative designs (Fig. 3, Row2) at realistic operating conditions. Authors intend to further utilize developed computational tools to propose advanced new design of a zero-leakage cylindrical seal .

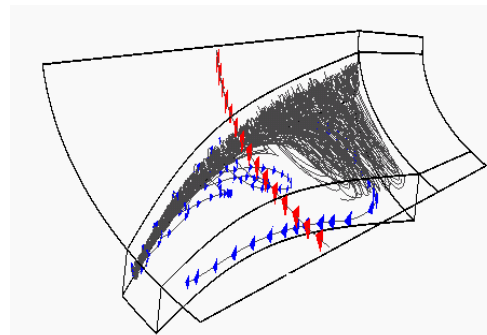


Fig. 6 Tornado-like flow formation in the groove
Arrows pointing in circumferential direction show direction of rotation. No external pressure gradient.

Results of the 3-D flow analysis are shown in Fig. 6. Note that vertical axis (z) was scaled by a factor of 10 (on all figures shown in this study) in order to be able to visualize the flow in the groove. This particular example shows fluid flow due to rotation only, no pressure gradient was imposed. Red arrows (Fig. 6) show the direction of the runner rotation and blue arrows show the recirculation flow structure in the groove. We can clearly see how the flow stream is entrained along the left groove side into the seal and how its rotational intensity grows, as it moves along the sidewall and further towards the dam. At the dam, it reaches full width of the spiral groove and part of it leaks (seal leakage) through the dam to the low pressure zone and part of it returns back along the other side of the groove. Such recirculation formation is due to inertial effects and can not be properly considered in a framework of Reynolds based lubrication theory [7-12].

To further expand on this finding we imposed a pressure difference of $3.5E5 \text{ Pa}$ (51 psig) between the outer and inner radii and performed computations for clockwise and counter-clockwise runner rotation. Results of this study are depicted in Figs. 6-8.

Opposite rotation, angular velocity $\omega = 2600$ rad/s. In this case flow component due to rotation hits the left sidewall, splitting in two directions (Fig. 7a). This is superimposed with the outer-to-inner radii flow direction, causing pressure hike shown in Fig. 7c. The reader can find the resulting flow visualization and related pressure distributions in Fig. 7(a,b,c). The force developed by the seal segment F_s in the vertical direction (load capacity) is equal to 324.3N and the leakage mass flow rate Q_s is equal to $19.041E-6$ kg/s. Total leakage flow Q will be equal to 8 Q_s , and total force F will be equal to 8 F_s (per geometry shown in Appendix 1) .

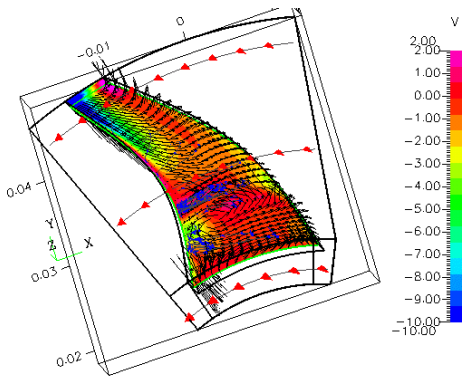


Fig. 7a Horizontal cross-section, vector plot

Tornado-like flow formation (as shown in Fig. 6) can also be found on Figs. 7b. Zones of positive and negative velocity (y-direction) indicate that part of the flow turns around and flows against the pressure gradient. For this particular design, size of this area of counterflow is very limited (compare Figs. 7a and 8a).

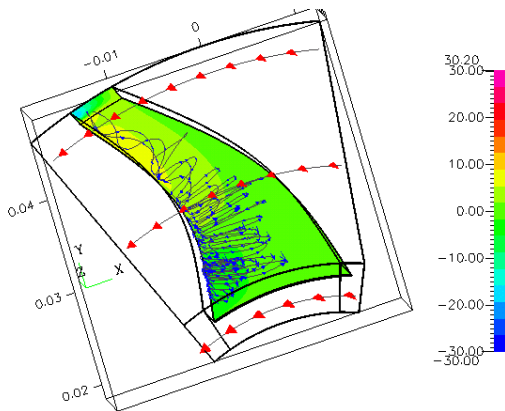


Fig. 7b Groove flow and recirculation

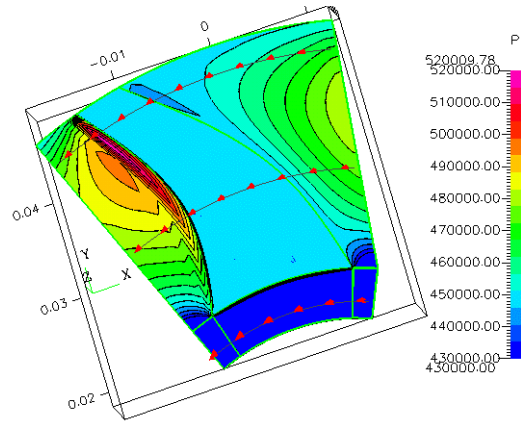


Fig. 7c Pressure distribution on the runner surface

Arrows pointing in circumferential direction show direction of rotation. XYZ coordinates are shown on the figure.

Aligned Rotation (shown in Fig 4), $\omega = -2600$ rad/s. In this case runners inward “pumping” action stimulates the flow to move continuously along the right sidewall. In Figs. 8 (a, b, c) the reader can find the respective flow visualization results and related pressure distributions. The total force developed by the seal segment in vertical direction (load capacity) is equal to 215.76N (x8 for total force along the circumference), while the leakage mass flow rate is $8.379 E-6$ kg/s. We can see that for the same operating conditions and characteristic seal ratios (gap/groove depths, land-to-groove areas, dam- to-groove lengths, etc.) groove layout, groove angle and orientation can considerably change leakage flow. In this particular case inward pumping action (aligned with rotation) produced 200% more efficient seal. Maximum peak pressure is 8% lower (compare Fig. 7b and 8c), which is due to “unfriendly” aerodynamic shape of the left boundary (Fig. 7c) and stronger stagnation effects. These effects, however, fail to produce required flow sealing effect. It is our hypothesis that sealing is predominantly due to flow stagnation near the dam. Reader can notice that for inward pumping resulting force F_s is smaller. This is due to reduction in overall mass flow rate. In order to adequately compare forces we need to change our model formulation. We shall use inlet flow boundary conditions instead of pressure boundary conditions. Presented results show that groove angle alignment can considerably affect load capacity and sealing efficiency of the spiral groove design. Aligned rotation (inward pumping) layout produces 200%

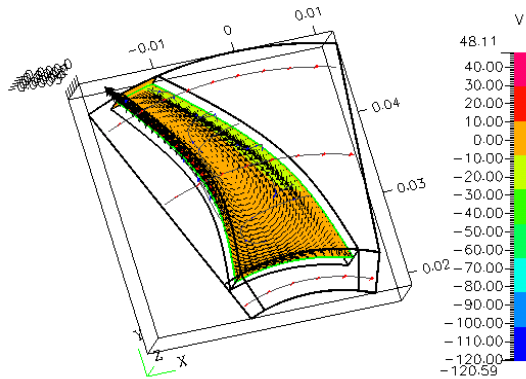


Fig 8a. Horizontal cross-section. Shows flow turn-around in the groove. Rotation from left to right.

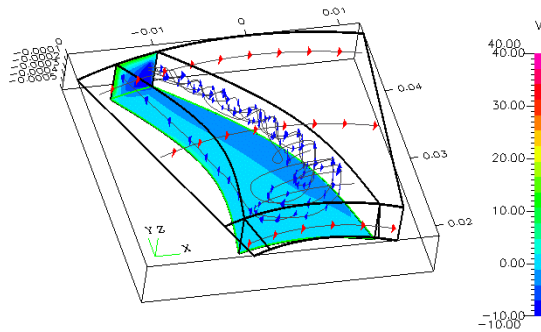


Fig. 8b Vortical flow structure. Dark color shows negative horizontal velocity component, light color shows positive. Positive direction heads out of the groove.

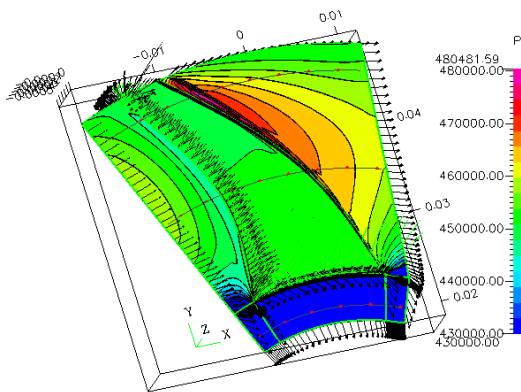


Fig. 8c Pressure Field on the surface of the runner (range shown 4.8E5 to 4.3E5 Pa). Flow vectors point to the flow direction.

reduction in the leakage flow. We also clearly demonstrated that at seal operating conditions flow separation and recirculation develops in the spiral

groove leading to complex 3D tornado-like vortex formation, which in turn considerably affects overall sealing efficiency.

CONCLUSIONS

The authors had successfully solved the full 3-D compressible Navier-Stokes flows in a realistic spiral groove seal configuration when the working fluid is a gas. The results clearly demonstrated the practical computational feasibility and technical need for such an approach. The seal flow formations are very complex in nature, and at the angular velocities used demonstrated strong inertial effects (Fig. 6-8), pointing to limitations of the Reynolds equation and narrow groove theory based approaches. Seal leakage flows were calculated and load carrying capacity was established for a given set of operating conditions. The results also showed that groove layout and direction of rotation can significantly impact leakage flow. Finally, the computational templates developed by the authors can be widely and easily utilized by industrial engineers.

REFERENCES

- [1] W. Shapiro, A. Artiles, B. Aggarwal, J. Walowit, M. Athavale, A. Przekwas, Numerical, analytical, experimental study of fluid dynamic forces in seals, interim rep. # 1, NASA Contract NAS3-25644, Dec. 1991, MTI 92TR6, Mechanical Technology Incorporated
- [2] J.H. Yohr, C.Y. Chow, Characteristics of Herringbone-Grooved, Gas Lubricated Journal Bearings, Trans. of ASME, Journal of Basic Engineering, Sep. 1965, p. 568-575
- [3] Malanoski, S.B., and Pan, C.H.T., 1965, "The Static and Dynamic Characteristics of the Spiral-Grooved Thrust Bearing", *ASME Journal of Basic Engineering*, pp. 547-558
- [4] Jed Walowit, Presentation of Computer Code SPIRALI for incompressible, turbulent, plane and spiral grooved cylindrical and face seals, Seals Flow Code Development-93, NASA CP 10136, Proceedings of a workshop held at NASA Lewis Research Center, Nov 3-4, 1993
- [5] G.G. Pechnt, J.P. Netzel, Design and Application of Non-contacting Gas Lubricated Seals for Slow Speed Services, STLE Presentation preprint No. 99-AM-19, Presented at 5th Annual Meeting, Las Vegas, Nevada, May 23-27, 1999

[6] J.A. Walowit, Users Manual for Computer Code SPIRALG Gas Lubricated Spiral Grooved Cylindrical and Face Seals, Rev July 1992, NASA Report, NAS3-25644, 91TM11

[7] M. Proctor, NASA Glenn Research Center <http://www.grc.nasa.gov/WWW/TurbineSeal/paper/s/99/19-proctor.pdf>

[8] Software for Analysis and Design of Turbomachinery Seals (GFACE,GCYL) <http://www.nasatech.com/Briefs/Dec98/LEW16582.html>

[9] L. San Andres, Spiral Groove Seal <http://metrib.tamu.edu/Software/SGFSdisclosure.htm>

[10] M. Rasaei and S.H. Winoto, Visualization in the Interface of a Noncontacting Mechanical Face Seal with Spiral Groove Pattern, [Journal of Flow Visualization and Image Processing](#), Volume 4, Number 2 (1997)

[11] Smalley A.J., The Narrow Groove Theory of Spiral Grooved Gas Bearings: Development and Application of a Generalized Formulation for Numerical Solution", ASME J. Lub. Techn v.94, 1, 1972, pp. 86-92

[12] P Song, C Kuangmin, A Model of Zero Pressure Difference and Zero Leakage for Non-contacting Spiral Groove Liquid Face Seals <http://www.bhrgroup.co.uk/confsite/fs-2home.htm> 16th International Conference FLUID SEALING *Successful Sealing*, Brugge, Belgium: 18-20 September 2000

[13] Launder, B.E., Leschziner, M., Flow in Finite-Width Thrust Bearings Including Inertia Effects II, Turbulent Flow, Trans. ASME, Journal of Lubrication Technology, July 1978, pp. 339—345

[14a] Braun, M.J, Dzodzo, M., "Effects of Hydrostatic Pocket Shape on The Flow Patterns and Pressure Distribution", International Journal of Rotating Machinery, Vol. I, No. 3-4, pp. 225-235, 1995

[14b] Braun, M.J., M. Dzodzo, "Three Dimensional Flow and Pressure Patterns in a Hydrostatic Journal Bearings Pocket", ASME Journal of Tribology, Vol. 119, No. 4, pp. 711-719, 1997

[15a] M. Braun, V. Kudriavtsev, A Numerical Simulation of a Brush Seal Section and Some Experimental Results, Journal of Turbomachinery, vol. 117, Jan 1995, p. 190-201

[15b] V.V. Kudriavtsev, M.J. Braun, "Interstage Disk-Cavity/Brush Seal Numerical Flow Visualization Study", International Journal of Turbo and Jet Engines, 13, 75-90 (1996)

[15c] V.V. Kudriavtsev, M.J. Braun, "Model Developments for the Brush Seal Numerical Simulation", Journal of Propulsion and Power", Vol. 12, No. 1, Jan-Feb, 1996, pp. 193-201

[16] Users Manual, CFD-ACE+ v.6.4, Jan. 29, 2001, also <http://www.cfdrc.com>

[17] Simulation Manager Manual, v. 6.4, Jan. 29, 2001, also <http://www.cfdcanada.com/sm.pdf>

APPENDIX 1

GUI for the SPIRAL Groove Seal Setup

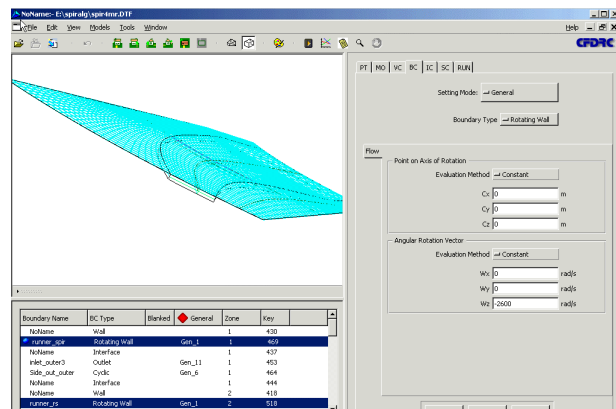
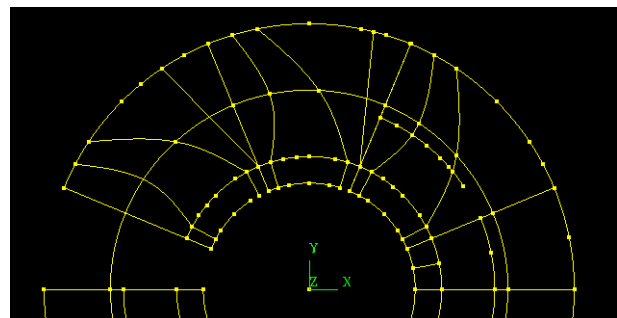


Figure shows "selected" runner surface and specified rotational velocity of 2600 rad/sec.

SPIRAL GROOVE WIREFRAME LAYOUT



Shows Geometry outline for considered seal segment. Eight full segments per circumference.